

## PERSPECTIVE OPEN



# Effect of climatic parameters on marine atmospheric corrosion: correlation analysis of on-site sensors data

Bahman Daneshian<sup>1</sup>✉, Daniel Höche<sup>1</sup>, Ole Øystein Knudsen<sup>2</sup> and Anders Werner Bredvei Skillbred<sup>3</sup>

A good understanding of influencing parameters is required to predict corrosivity in marine and coastal environments. This study investigated the influences of real-time data of (i) air temperature, (ii) sensor surface temperature, (iii) relative humidity, (iv) precipitation, and (v) wind on steel corrosion via data analysis. The results revealed that the time when the sensor surface temperature is below the dewpoint temperature reveals the best correlation with corrosion. Wind speed above  $5 \text{ m s}^{-1}$  also correlated with corrosion. At the test site, most of the corrosion occurred during autumn and winter, due to more water condensation and more wind. During spring and summer, there was little corrosion, due to little condensation and dry surfaces.

*npj Materials Degradation* (2023)7:10; <https://doi.org/10.1038/s41529-023-00329-6>

## INTRODUCTION

Steel constructions are protected from corrosive marine atmospheres by heavy-duty paint coatings, typically based on epoxy binders<sup>1</sup>. One of the most important parameters with respect to coating durability and lifetime is the corrosivity of the exposure environment<sup>2</sup>. This is also one of the main parameters for selecting protective coating systems<sup>3</sup>. A reasonable estimate of corrosivity is therefore important with respect to coating selection and its subsequent durability. Atmospheric corrosivity on a specific site is determined by exposing steel specimens for 1 year and measuring mass loss, according to ISO 9226<sup>4</sup>. In ISO 9223<sup>5</sup>, a dose-response model for calculating corrosivity is given, based on average daily chloride deposition rate, average daily sulfur oxide deposition rate, temperature, and relative humidity. Deposition rates of sulfur oxide and chloride are not readily available, though, which limits the usefulness of the model. A simpler but still reliable method for estimating corrosivity on a specific site is desired, both for advising coating selection and for estimating coating lifetime. The objective with this work was to investigate the effects of various climatic parameters on corrosion, for potential use in a future corrosivity model based on such parameters.

Several studies have been presented regarding the influence of atmospheric parameters on corrosivity. Recently, Li et al. measured instantaneous corrosion rate at six different locations and correlated corrosivity with weather data via machine learning<sup>6</sup>. They concluded that (i) wind speed, (ii) precipitation and (iii) relative humidity are the most important environmental parameters for corrosion rate, while chloride deposition, air temperature, and deposition of sulfur dioxide and nitrogen dioxide had little influence. The reported low influence of chloride and sulfur dioxide is surprising, and in contradiction with other studies<sup>7–9</sup>. Previous field testing, including the ISOCORRAG project that resulted in the ISO 9223 model, concluded that both chloride and sulfur dioxide deposition have a significant influence on steel corrosion<sup>8,10,11</sup>.

For marine and coastal environments, chlorides are expected to be a more important driver for corrosion than sulfur dioxide, since it is present in much higher concentrations. The effect of chloride on corrosion has been studied extensively for various metals in

the laboratory. Several investigations on the impact of airborne salt on the corrosion rate of steel have also been published<sup>12–14</sup>. Direct measurement of atmospheric chloride deposition is not straightforward, so replacing this parameter with more accessible weather parameters will simplify the assessment of corrosivity. Recent studies have also shown that wind conditions significantly affect salt deposition in marine and coastal environments<sup>13,15,16</sup>. Hence, wind data may be used to estimate corrosivity, along with other weather parameters like air temperature and relative humidity, instead of chloride and sulfur dioxide deposition used in ISO 9223.

This paper presents a study where sensors were used to measure corrosion rate and atmospheric parameters simultaneously with 30 or 60 minutes resolution. The sensor data enables correlation studies between corrosion and weather conditions. Sensor data were obtained continuously during 1 year, and based on this data set, the single and interactive influences of the atmospheric parameters on the corrosion rate and the corrosion progress were studied.

## RESULTS

### Time-resolved corrosion measurements and weather parameters

The data set consisted of 16785 rows with time-stamped measurements of air temperature ( $T_a$ ), surface temperature ( $T_s$ ), relative humidity (RH), and free corrosion current ( $I_c$ ) obtained from CorRES sensor plus 8766 rows of the precipitation, wind speed and wind direction data obtained from the meteorological stations with 1 hour resolution. Figure 1 shows the collected raw data.

An inverse behavior between the surface temperature and the relative humidity is evident in Fig. 1a. In addition, comparing the surface temperature with the air temperature in Fig. 1a reveals that surface temperature can increase even up to  $30^\circ\text{C}$  in February. The precipitation data analysis in Fig. 1b shows little precipitation in this region. The analysis of the wind speed data in Fig. 1c shows presence of severe winds with speeds above  $20 \text{ m s}^{-1}$  in October–April period, while the maximum wind speed remains below  $15 \text{ m s}^{-1}$  in May–September period. The wind

<sup>1</sup>Helmholtz-Zentrum Hereon, Max-Planck-Straße 1, 21502 Geesthacht, Germany. <sup>2</sup>SINTEF Industry, Richard Birkelandsvei 2B, 7465 Trondheim, Norway. <sup>3</sup>Jotun AS, Hystadveien 167, 3202 Sandefjord, Norway. ✉email: bahman.daneshian@hereon.de

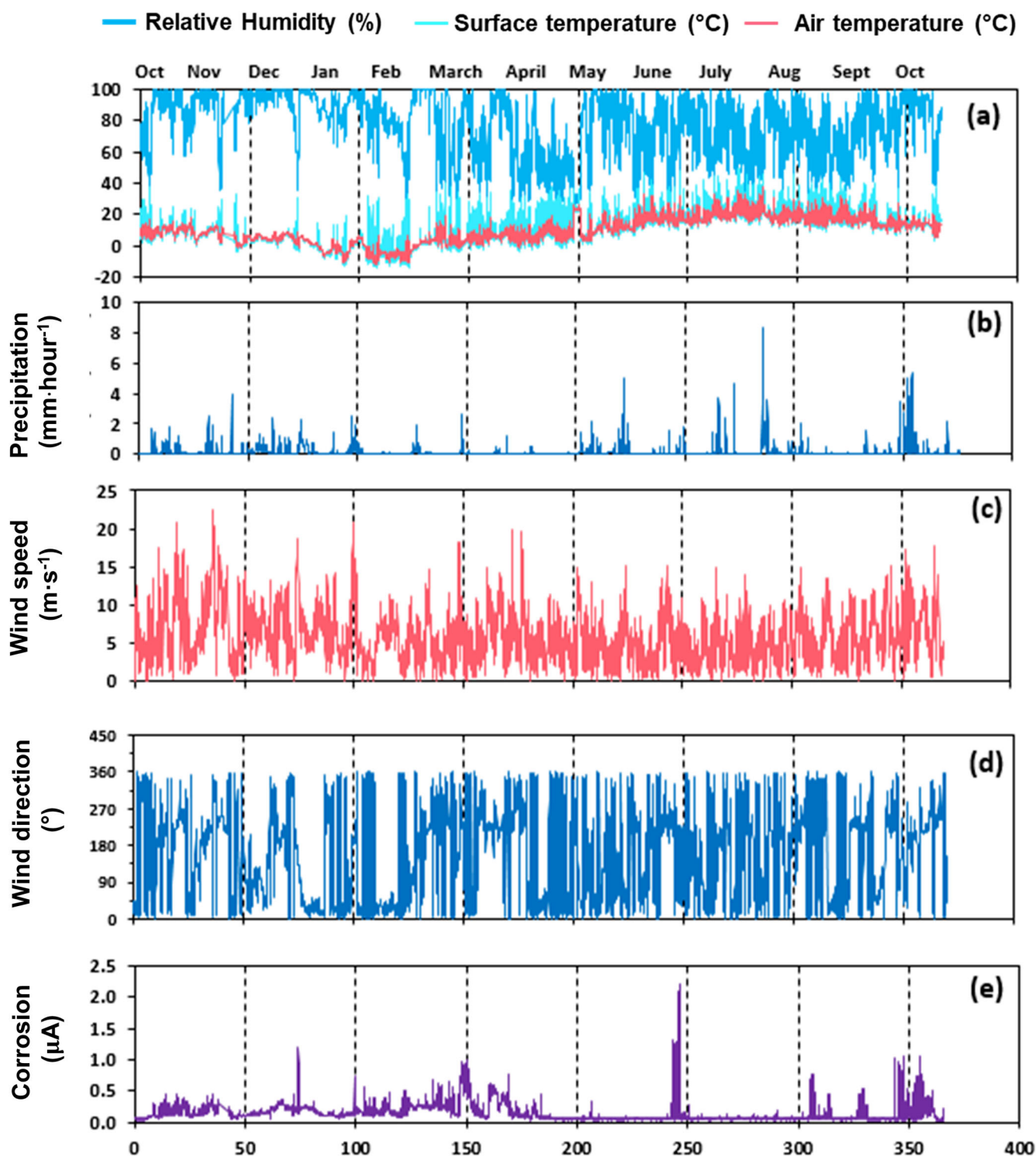


**Fig. 1 Raw data.** Plots of **a** air temperature, surface temperature, relative humidity with 30 minutes resolution, **b** precipitation with 1 hour resolution, **c** wind speed with 1 hour resolution, **d** wind direction with 1 hour resolution and **e** corrosion rate with 30 minutes resolution during 1 year from 14 October 2020 until 14 October 2021.

direction data analysis in Fig. 1d also shows that this data type is very dynamic even at a daily scale, making analyzing the wind direction data difficult. Most data oscillations are, however, observed around  $0^\circ$ ,  $270^\circ$ , and  $360^\circ$  directions. At the end, analysis of the free corrosion current data in Fig. 1e shows that corrosion mainly occurred in October–March period, while corrosion was limited in the summertime. The data set of Fig. 1 was created from

14 October 2020 until 14 October 2021, although the sensor was deployed at the site from the 1 April 2019. In fact, the data recorded until 14 October 2020 was discarded from the data set due to some technical problems. Hence, the corrosion reported here does not include the high initial corrosion rates.

Figure 2 shows the recorded instantaneous and accumulated corrosion during the 1-year test period from 14 October 2020 until

14 October 2021. During the autumn and winter months from October to end of March, corrosion was occurring continuously. In April corrosion decreased and during May, June, and July there was almost no corrosion. The high corrosion in mid-June coincides with a few consecutive days of 10–15 m s<sup>-1</sup> wind that may have caused significant salt deposition on the panels, see Fig. 1c. Figure 1b shows that there was little rain during these days, so any salt deposits were not washed from the sensor surface. In August and September increasing corrosion was registered. The low corrosion during summer can probably be attributed to a pleasant summer climate at the test location with sunny, dry weather and relatively low wind speeds, as Fig. 1 indicates.

### Effect of temperature and relative humidity on corrosion

Figure 3a, b show average free corrosion current as function of atmospheric temperature and sensor surface temperature. The sensor surface temperature in Fig. 3b was higher than the atmospheric temperature, up to 50 °C due to heating by the sun. Average relative humidity is given in the same plots. The average corrosion and RH values were calculated for each temperature span of 0.1 °C. A substantial decrease in corrosion can be seen at air and surface temperatures above 15 °C. Similarly, the relative humidity decreased noticeably at air and surface temperatures above 15 °C too. The free corrosion current was almost negligible at air and surface temperatures above 20 °C. The decrease in

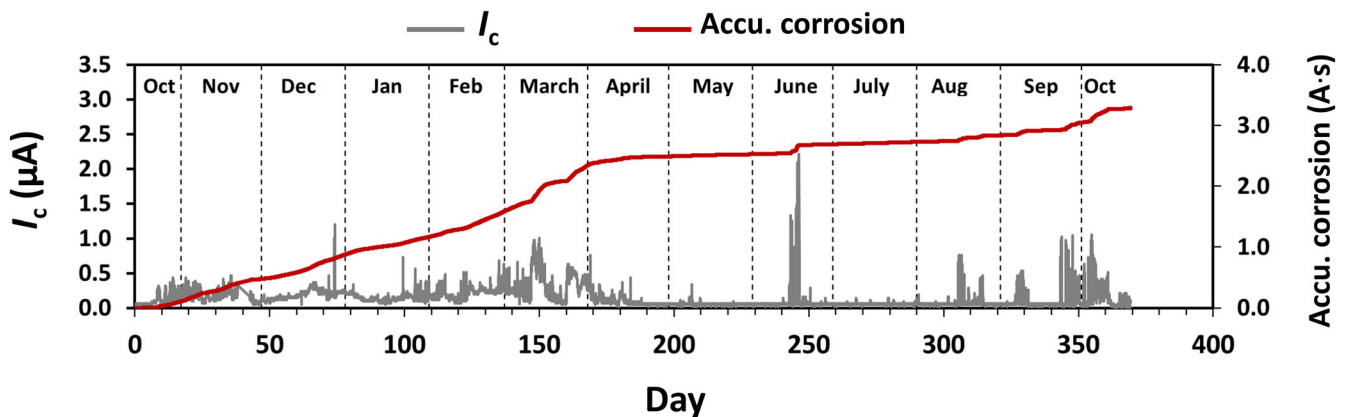
corrosion and relative humidity above 15 °C is attributed to warm and dry weather at such temperatures for this site. The drop in corrosion rate around 10 °C may have been accidental but will be discussed in relation to precipitation below.

The free corrosion current also decreased at temperatures below zero, although the relative humidity remained at ~80%. This drop can reasonably be attributed to generally decreased reaction rates at low temperature, or ice formation on the samples. The diagrams show that corrosion mainly occurred at temperatures between -5 and 15 °C, when the relative humidity was above 80%.

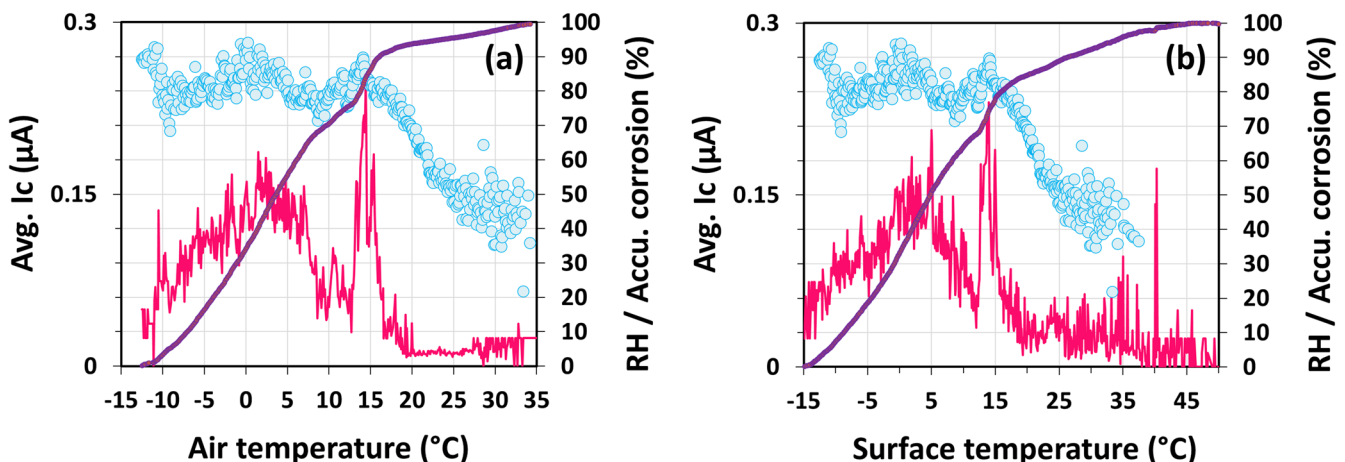
### Correlation between precipitation and corrosion

Figure 4a illustrates the influence of precipitation on average corrosion at the test site. The maximum daily precipitation at this site was about 6 mm during the year of measurement. Corrosion rate plotted against precipitation shows a continuous decrease. The mechanism behind the effect would be that the rain washes salt away from the surface of the corrosion sensor. The corrosion sensor was tilted 45 °, which facilitates a washing effect of water droplets running across the surface.

In Fig. 4b total precipitation is plotted in the corrosion versus air temperature diagram from Fig. 3a. The trendline of precipitation versus atmospheric temperature shows a maximum at 10 °C. This maximum coincides with the minimum point in the Avg.  $I_c$  curve.



**Fig. 2 One-year corrosion.** Corrosion current ( $I_c$ ) and accumulated corrosion (Accu. corrosion) during the 1-year test period from 14 October 2020 to 14 October 2021.



**Fig. 3 Effect of temperature.** Influences of atmospheric temperature (a) and the sensor surface temperature (b) on the average free corrosion current (the red curve), accumulated corrosion (the purple curve) and the relative humidity (the blue dots). The average values were calculated for temperature intervals of 0.1 °C.

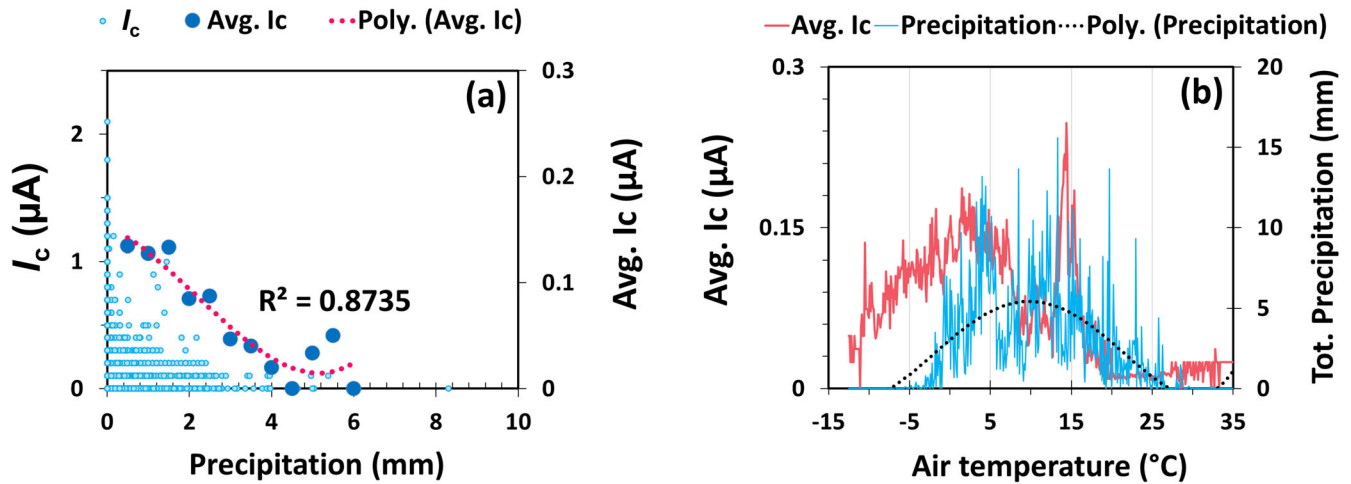


**Fig. 4 Effect of precipitation.** Influence of precipitation on corrosion. **a** Free corrosion current ( $I_c$ ) (the light blue dots) was plotted as function of precipitation, and average free corrosion current (Avg.  $I_c$ ) (the dark blue dots) was plotted for 0.5 mm intervals of precipitation. **b** total precipitation (the blue curve) and average free corrosion current (the red curve) were plotted versus the air temperature.

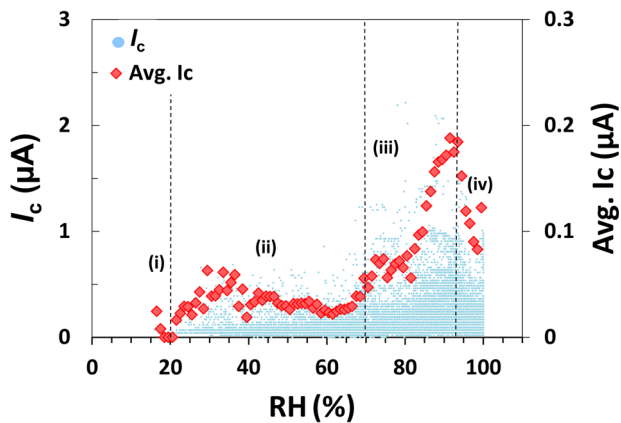


**Fig. 5 Effect of relative humidity.** Influence of relative humidity (RH) on free corrosion current ( $I_c$ ) (blue dots) and on the average free corrosion current (Avg.  $I_c$ ) (red dots).

This indicates that the observed decrease in corrosion between 5  $^{\circ}\text{C}$  and 15  $^{\circ}\text{C}$  can be attributed to the influence of precipitation. Due to the limited range of daily precipitation, it is not reasonable to make general conclusions about the influence of precipitation on corrosion, though.

#### Correlation between relative humidity and corrosion

In Fig. 5 the free corrosion current ( $I_c$ ) is plotted versus relative humidity (% RH), as well as the average free corrosion current (Avg.  $I_c$ ) was calculated for every 1% increment of RH. The diagram shows four ranges of RH with different effects on corrosion: (i) at RH < 20%; corrosion is negligible. (ii) Corrosion is low and independent of RH between 20–70%. (iii) Corrosion increases rapidly between 70 and 93% RH, (iv) A significant drop in corrosion is seen at RH higher than 93%.

The rapid increase in corrosion rate above 70% RH in (iii) is attributed to condensation of water on the corrosion sensor and absorption of air humidity by salt deposits. NaCl is generally dissolved above 70% RH<sup>13,17</sup>. The observed rapid decrease in corrosion at RH > 93% in (iv) can be explained by a washing effect from rain or condensed water running across the sensor<sup>18</sup>. About 45% of the precipitation was registered during periods with RH > 93%.

#### Correlation between time of wetness and corrosion

The effects of atmospheric temperature and relative humidity were studied separately above, but their combined effect should be considered since this affects condensation on surfaces. For this, the parameter time of wetness (TOW) is often applied. TOW has been defined as when RH  $\geq$  80% and  $T_a > 0^{\circ}\text{C}$ <sup>19</sup>, and this definition is also applied here. In Fig. 6, the accumulated TOW is plotted with the accumulated corrosion. Each corrosion measurement was multiplied by the time since last measurement, to compensate for any variation in logging frequency. The accumulated corrosion is given in As or Coulombs. Comparing accumulated TOW and accumulated corrosion, shows that trend of the TOW curve is very similar with the trend of the corrosion curve only from October to end of February. In fact, the accumulated TOW shows almost a linear trend and therefore does not correlate with the high corrosion rate measured in March, nor the low corrosion rate from April to August.

#### Effect of dewpoint on corrosion

Dewpoint is a more reliable parameter for determining the presence of condensed water on surfaces<sup>18</sup>. The dew point temperature is calculated from the atmospheric temperature ( $T_a$ ) and the relative humidity (RH) parameters as per Eq. (1)<sup>20</sup>, where  $\beta$  and  $\lambda$  are 17.62 and 243.12  $^{\circ}\text{C}$ , respectively.

$$T_{dew}(T_a, RH) = \bar{\lambda} \cdot \frac{\ln\left(\frac{RH}{100\%}\right) + \frac{\beta \cdot T_a}{\lambda + T_a}}{\beta - \ln\left(\frac{RH}{100\%}\right) - \frac{\beta \cdot T_a}{\lambda + T_a}} \quad (1)$$

Time of condensation (TOC) was calculated as the time when the sensor surface temperature ( $T_s$ ) is below the dew point temperature ( $T_s \leq T_{dew}$ ). Figure 7 shows the instantaneous variations of accumulated time of condensation and the accumulated corrosion over the time. The plot shows that during the period with high corrosion rate from October to March, the accumulated time of condensation was also high, while the period with low corrosion rate from April to August showed low accumulated time of condensation too. The observed correlation seems much better compared with the accumulated time of wetness in Fig. 6. Since unlike the linear trend of accumulated time of wetness in Fig. 6, here both curves show a similar nonlinear trend.

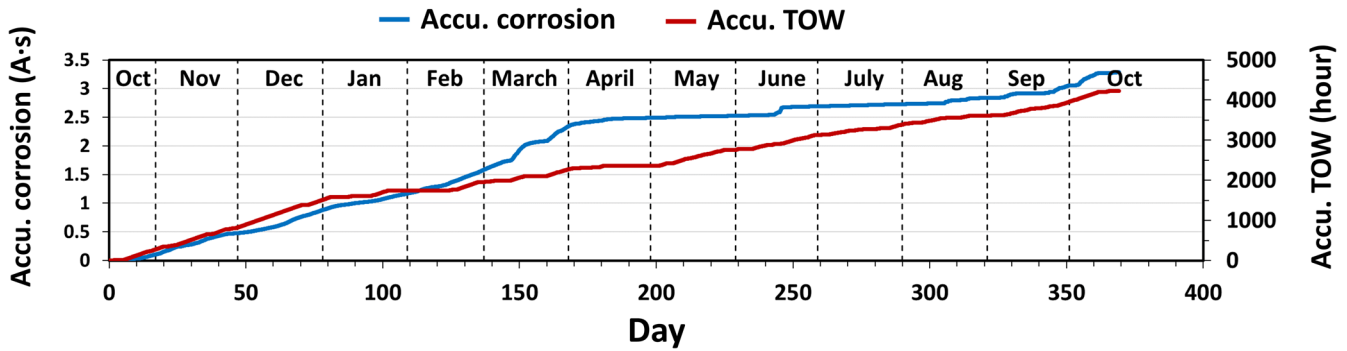


**Fig. 6 Correlation (time of wetness, corrosion).** Accumulated time of wetness was plotted with the accumulated corrosion during the test. TOW was defined as the atmospheric temperature was higher than 0 °C and the relative humidity was equal to and above 80%.

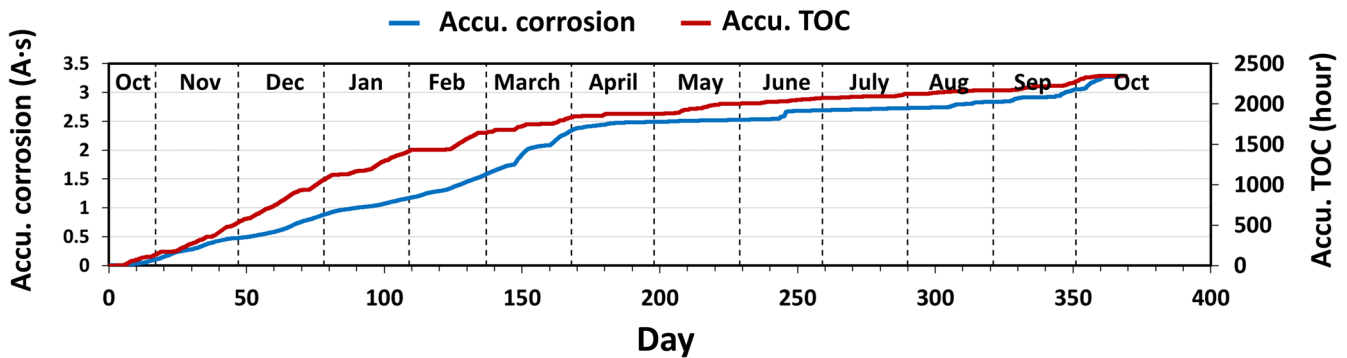


**Fig. 7 Correlation between condensation and corrosion.** Cumulative time of surface temperature  $T_s$  below the dew point temperature ( $T_s \leq T_{dew}$ ) plotted with accumulated corrosion during the 1-year test period.

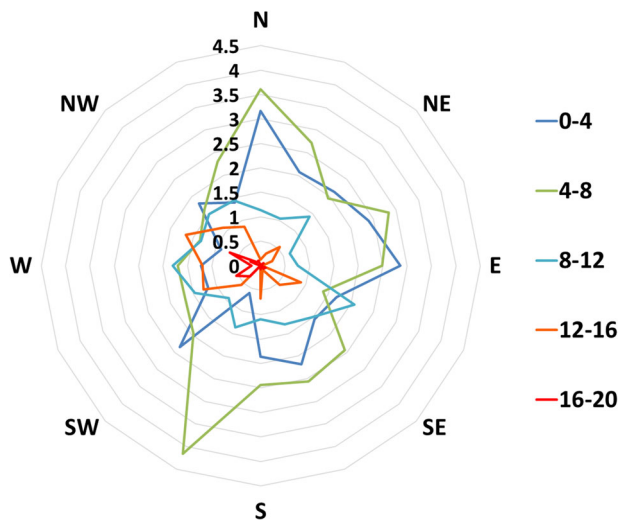


**Fig. 8 Wind rose.** Wind rose for the 1-year test period, based on wind data from Svenner lighthouse, ~8 km distance from the corrosion test site.

### Effect of wind on corrosion

The wind data was collected from Svenner Lighthouse where the Norwegian Meteorological Institute measures wind. The lighthouse is ~8 km distance from the corrosion test site, with open sea between. Hence, it is reasonable to assume that the wind at the test site is similar to the wind at the lighthouse. Figure 8 shows a wind rose plotted from the wind data. The dominating wind directions are between north and south-west, which correlates

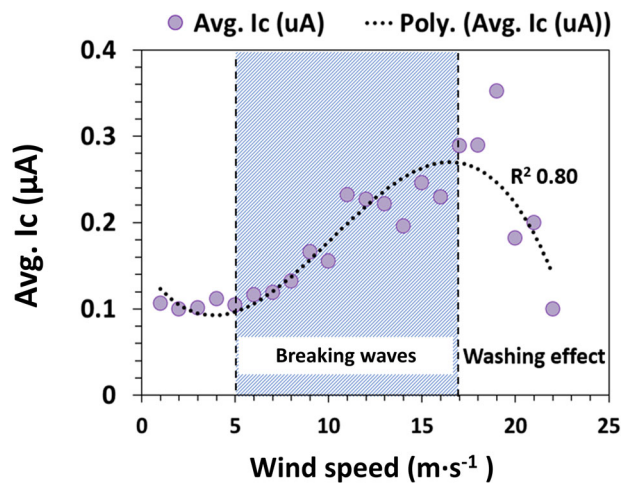


**Fig. 9 Effect of wind speed.** Average free corrosion current (Avg.  $I_c$ ) for each  $1 \text{ m s}^{-1}$  increment in wind speed plotted versus the wind speed. The fitted line is a third-order polynomial.

with the orientation of the coastline at the test location. The test location is on the east side of a fjord. Hence, the winds mainly blow from the fjord towards the shoreline. Therefore, adjusting the wind data by its direction, i.e., disregard winds from land, did not improve correlation to corrosion.

Figure 9 shows the influence of wind speed on the average free corrosion current. The diagram shows that the corrosion rate significantly increases with increasing wind speed from 5 to  $17 \text{ m s}^{-1}$ . The threshold wind velocity of  $\sim 5 \text{ m s}^{-1}$  may be attributed to formation of breaking waves. Breaking waves

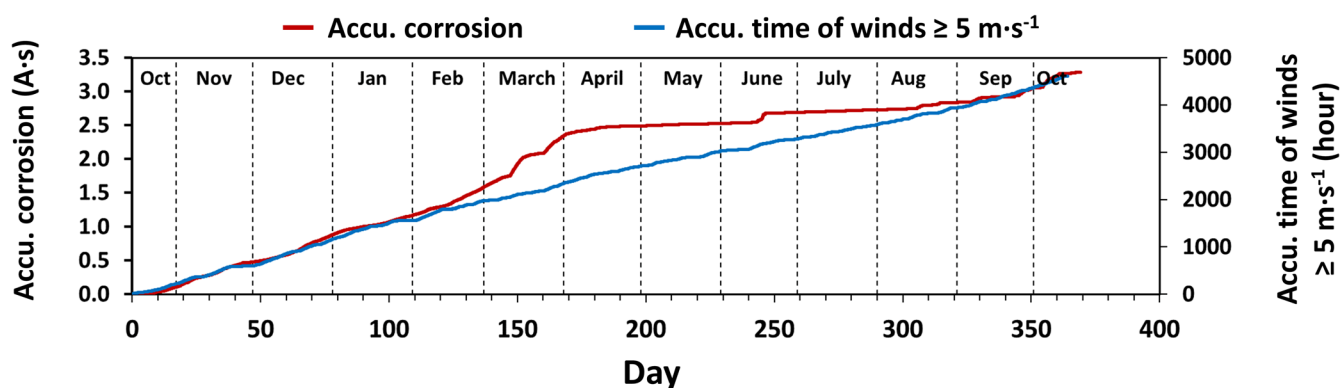


**Fig. 10 Correlation between wind and corrosion.** Correlation between accumulated time of winds, for winds  $\geq 5 \text{ m s}^{-1}$ , in hours and accumulated corrosion.

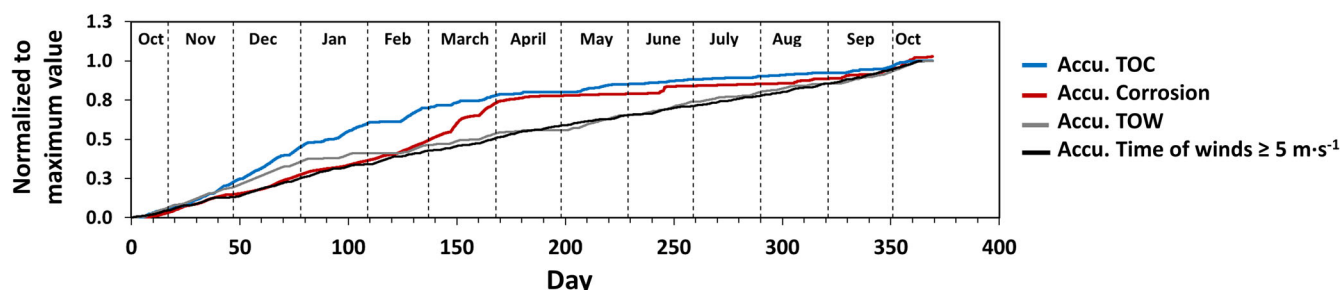


**Fig. 11 Comparison between all correlations investigated.** Correlation between accumulated corrosion with (i) accumulated time of condensation, (ii) accumulated time of wetness and (iii) accumulated time of winds, for winds  $\geq 5 \text{ m s}^{-1}$ .

produce the sea salt particles in the air via bubble bursting by different mechanisms. The low corrosion rate above  $17 \text{ m s}^{-1}$  may be attributed to a washing effect of seawater splashing onto the sensor due to large waves. Another explanation may be rain coinciding with high wind, also resulting in a washing effect. Since the number of data points at such high wind speeds was relatively low, the effect of accidental variation or outliers cannot be excluded either.

Figure 10 shows correlation between accumulated time of the wind speeds  $>5 \text{ m s}^{-1}$  and the accumulated corrosion. Although this figure shows very good correlation between the accumulated wind duration and accumulated corrosion from in October–February, there are also periods with low correlations, e.g., in March–August where the high corrosion rate is not reflected by much wind durations.

Figure 11 was plotted for detail study of the correlation between the accumulated corrosion with concepts like (i) the accumulated time of condensation, (ii) the accumulated time of wetness, and (iii) the the accumulated winds durations. For this purpose, first the maximum values of the accumulated corrosion, accumulated time of condensation, accumulated time of wetness and the accumulated winds durations (for wind speed above  $5 \text{ m s}^{-1}$ ) were calculated. Then the data were divided to their own maximum values to provide data between 0 and 1 ready for easy comparison. The assessment results in this figure shows that the accumulated time of condensation better predicts the accumulated corrosion values as well as the corrosion rate (slope of the accumulated corrosion curve) rather than the others. While accumulated time of wetness and accumulated wind duration show almost a similar linear trend.

In order to assess the correlation between the accumulated corrosion with (i) time of wetness, (ii) wind duration, and (iii) the condensation time, Pearson coefficients<sup>21</sup> of correlation were calculated. The Pearson coefficient between the accumulated

corrosion and the accumulated time of winds was 0.98, for winds with speeds above  $5 \text{ m s}^{-1}$ . The Pearson coefficient between the accumulated corrosion and the accumulated condensation time was 0.98, which shows a better linear correlation than the Pearson coefficient between the accumulated corrosion and the accumulated time of wetness (0.96).

Even though this analysis shows some strong correlations, it must be emphasized that the provided data set comes from only one specific coastal test site. The results indicate that time of condensation and winds above  $5 \text{ m s}^{-1}$  have a strong effect on corrosivity. However, results from more test sites must be collected before we can make general conclusions.

## DISCUSSION

The study of how weather and climatic conditions affect corrosion in the field is complicated by the simultaneous effect of several parameters. In the laboratory, the Arrhenius model<sup>17,22</sup> will describe the impact of temperature on the corrosion rate, when all other parameters can be kept constant. However, in an outdoor environment, parameters like wind, sunshine and precipitation will vary and also affect the corrosion rate. Hence, the field corrosion rate will not follow the Arrhenius function of temperature, as can be seen in Fig. 3. Another complicating factor in the analysis of instantaneous corrosion in the field, is the constant variation of the parameters<sup>23</sup>. The conditions that affect corrosion are in constant dynamic variation. This may result in time lags between the state of the parameters and the corrosion rate. E.g. the wind may deposit salt on the corrosion sensor, but the required humidity for corrosion may first appear much later. Previous work has to a large extent focused on annual averages of the key parameters, e.g., the ISOCORRAG project<sup>8</sup>, which eliminates this problem. On the other hand, by this approach a detailed understanding of the effect of weather and climate on corrosion was impossible.

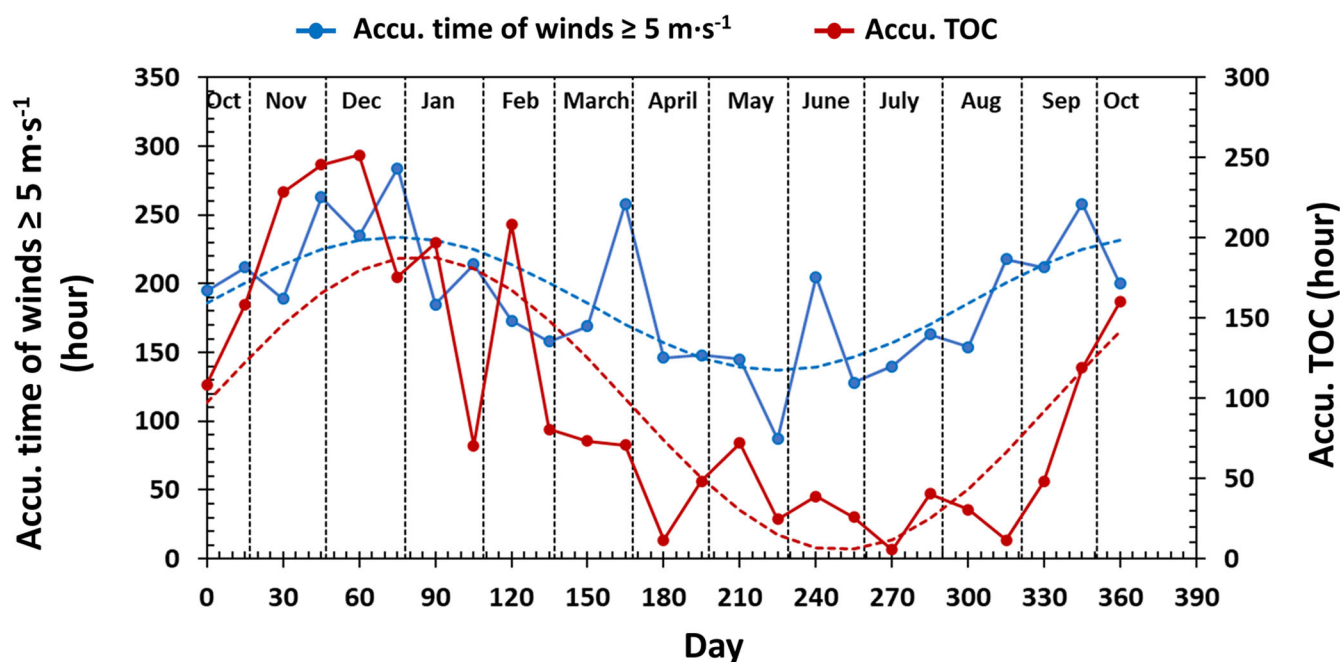


**Fig. 12 Seasonal variation of wind and condensation.** Plots the accumulated time of winds  $\geq 5 \text{ m s}^{-1}$  and time of condensation in every 15 days. The dashed curves represent sinusoidal regression models with  $R^2$  values of 0.48 (blue curve) and 0.63 (red curve), respectively.

Temperature plays a vital role for corrosion by affecting the surface electrolyte and generally affecting reaction rates due to their activation energy. According to Fig. 3, most of the corrosion occurred between  $-5$  and  $15^\circ\text{C}$ . The average temperature during the test period at the site was  $12.1^\circ\text{C}$ , so this temperature range also includes a large fraction of the measurements. The results showed that the sensor surface temperature ( $T_s$ ) reached  $50^\circ\text{C}$  in the summer and  $30^\circ\text{C}$  in the winter due to sunshine directly on the sensor panels. Hence, sunlight may effectively dry out the surface electrolyte and suppress corrosion. In the winter, heating by sunlight can also melt ice or increase temperature into a more active range and increase corrosion. Therefore, attention to the sensor surface temperature is recommended for more detail corrosion prediction.

The temperature measurements also showed that the effects of atmospheric or surface temperature on corrosion are nonlinear. Previous studies have claimed that daily average atmospheric temperature is not an essential parameter for atmospheric corrosion<sup>15,17,23–26</sup>, but this study showed that temperature will affect corrosion by its effect on (i) evaporation, (ii) condensation and (iii) freezing. Whether temperature should be included in a corrosion model based on climatic parameters, or if its influence is better represented by other parameters, is beyond the scope of this work.

The results showed a significant increase in corrosion when the relative humidity exceeded 70% (Fig. 5). Relative humidity has previously been considered as one of the most important environmental factor affecting atmospheric corrosion<sup>22</sup>. Since the presence of water is a fundamental condition for corrosion, this is not surprising. Some studies have concluded that almost no atmospheric corrosion can occur, when the relative humidity is below 70%, unless the surface is contaminated by salts<sup>24,27</sup>. Studies have showed that when the surface is covered by sea salts or corrosion products, corrosion may occur at much lower relative humidity<sup>25</sup>. However, salt also affects corrosion by the effect of chloride on the composition of partly protective surface oxides<sup>9</sup>. The fact that little corrosion was registered below 70% RH in this study, can therefore not be taken as an indication that salt had little effect on the corrosion.

The time of condensation was calculated in this study by the time when the surface temperature was equal to or below the dew point temperature. The time of condensation showed a significantly better correlation with corrosion than the time of wetness (Fig. 6 and Fig. 7) that frequently has been used before. However, calculating time of condensation requires frequent logging of the sensor surface temperature, besides the air temperature and relative humidity that are applied in the time of wetness calculation.

Wind creates the waves that bring sea salt particles into the air, and it blows the sea salt onto the construction<sup>9,15</sup>. Sea aerosols are primarily produced by braking waves, and the threshold wind speed for braking waves is in the order of  $7 \text{ m s}^{-1}$  on the open ocean<sup>26</sup>. The results from this study showed that at wind speeds above  $5 \text{ m s}^{-1}$ , corrosion rate increased with increasing wind speed, which correlates well with the threshold wind speed for braking waves. Morcillo et al. has earlier suggested a  $3 \text{ m s}^{-1}$  threshold wind speed for increased corrosivity, but this study indicates that the threshold is higher than this<sup>15</sup>.

Accumulated time of winds (for wind speeds equal and above  $5 \text{ m s}^{-1}$ ) showed a similar trend as accumulated corrosion, see Fig. 10, indicating that this parameter correlates well with the corrosion. Adjusting the wind effect by taking wind direction into account, i.e., only including winds blowing from the sea towards the samples, did not improve the correlation to corrosion. The wind measurements were logged as hourly averages, which means that a certain variation in wind direction was included in all the measurements. Even when the hourly average say that the wind blows from land, there may be shorter periods with wind from the sea. Also, the wind on the site is mainly blowing from the sea towards shore, which means that excluding winds from land would only take out a limited fraction of the wind data and have a limited effect on the calculations.

Most of the measured corrosion occurred during the autumn and the winter. There was very little corrosion during the spring and summer, see Fig. 1e and Fig. 2. This issue is attributed to (i) the longer accumulated time of condensation and (ii) more frequent winds speeds  $>5 \text{ m s}^{-1}$ . In Fig. 12, the accumulated time of condensation and time of winds  $>5 \text{ m s}^{-1}$  are plotted for every

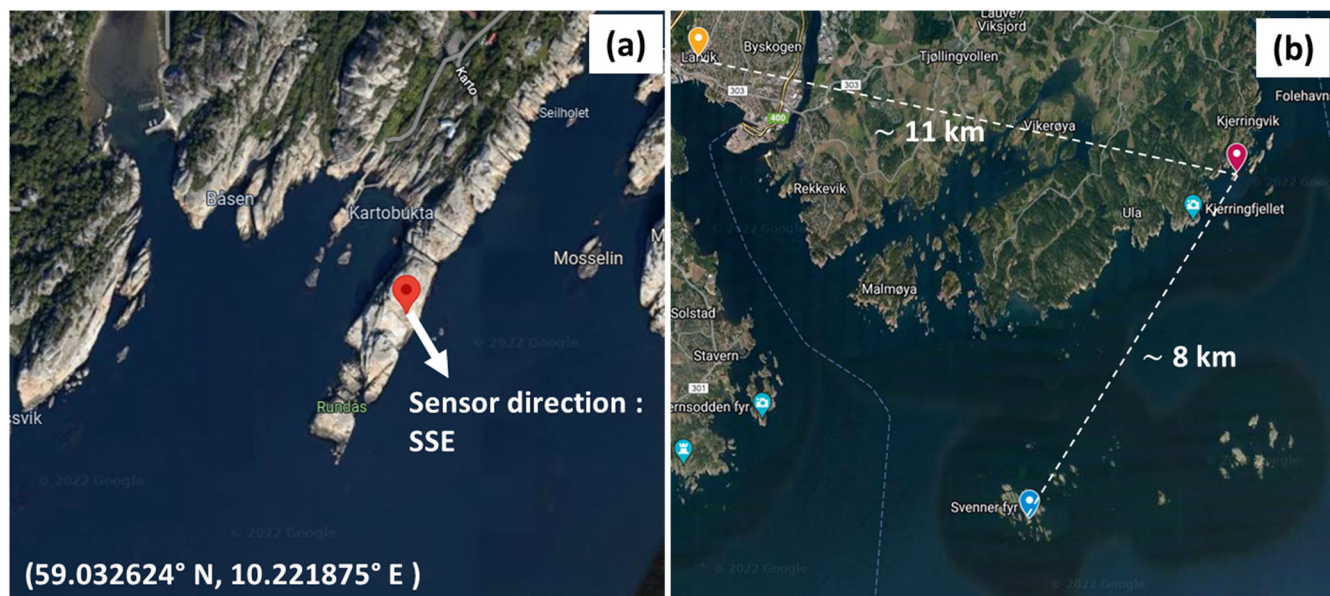


**Fig. 13 Locations of site and meteorological stations.** Location of the test site on the east side of the Oslo fjord (a) and the distances between the test site (pink pin), the Svenner lighthouse (blue pin) and the Larvik site (orange pin) in b.

15 days. Although both time of condensation and time of wind  $>5 \text{ m s}^{-1}$  show differences between winter and summer, the time of condensation shows the largest difference. Figure 12 can also explain the observed high corrosion rate in mid-June (about 240 days) in Fig. 1e and Fig. 2. Several consecutive days with strong winds in mid-June is shown by a peak in the wind curve at 240 days in Fig. 12, which caused deposition of sea salts on the sensor panel and increased the corrosion (see Fig. 1c also).

Precipitation resulted in reduced corrosion rate on the sample, probably due to a rinsing effect, where the rain washed salt deposits from the surface (Fig. 4). Similarly, relative humidity above 93% also resulted in decreasing corrosion rate (Fig. 5). The latter may be due to condensation of water on the sample which could have resulted in formation of droplets that run down the surface of the sample, creating the same rinsing effect. In 45% of the measurements of relative humidity above 93%, rain was also registered, so part of the effect was due to rain. We can therefore not say for certain that high humidity had a washing effect on the surface.

The reduced corrosion rate around  $10^\circ\text{C}$  (Fig. 4b) is attributed to rain, since much of the rain was recorded around this temperature. However, based on this data set alone, this should only be regarded as a hypothesis. Data from more test sites will be required before we can conclude on this.

## METHODS

### Data collection

A CorRES sensor from Luna Innovations was exposed at a coastal site at Kjerringvik in southern Norway- red pin in Fig. 13a. Information about precipitation was collected from Larvik (orange pin in Fig. 13b), while wind speed and direction were collected at Svenner lighthouse (blue pin in Fig. 13b). Both locations are meteorological stations operated by the Norwegian Meteorological Institute (met.no), and  $\sim 8$  and  $11 \text{ km}$  in direct line from the test site. There is open water between Svenner lighthouse and the test site, so the prevailing wind directions should be quite similar at both locations. The GPS coordinates of the test site, the Svenner lighthouse, and Larvik are  $(59.032624^\circ \text{ N}, 10.221875^\circ \text{ E})$ ,  $(58.9692^\circ \text{ N}, 10.1480^\circ \text{ E})$  and  $(59.0538^\circ \text{ N}, 10.0295^\circ \text{ E})$ , respectively.



**Fig. 14 The sensor package.** The CorRES sensor mounted at Kjerringvik in Norwayface toward the sea (southeast) tilted  $45^\circ$  from horizontal.

First-year corrosion was measured according to ISO 9226 in 2019–2020 and in 2021–2022, giving  $137 \mu\text{m}$  and  $196 \mu\text{m}$ , respectively. Hence, corrosivity on the site is category C5. The samples were exposed very close to the sea, so the high corrosivity at this site is governed by chloride deposition as per ISO 9223. According to Norwegian Institute for Air Research, the deposition of sulfur at the test site is in the order of  $200 \text{ mg/m}^2/\text{year}$ <sup>28</sup>, so we expect a little effect of  $\text{SO}_2$ .

### Sensor setup

The CorRES sensor setup used in this study consisted of a docking platform and two sensor panels (Fig. 14). One panel contains the weather sensors and measures surface temperature ( $T_s$ ), air temperature ( $T_a$ ), and relative humidity (% RH)<sup>29</sup>. The CorRES sensor data were logged with 30 minutes resolution. This sensor also measures the surface conductivity that was eliminated from this study. The other panel has a carbon steel



**Table 1.** Parameters measured by the CorRES panels.

Parameters	Symbol	Method	Range Min.	Range Max.	Units	Sensor excitation
Surface temperature	$T_s$	Thermistor <sup>30</sup>	−40	+85	°C	DC current
Air temperature	$T_a$	Thermistor <sup>30</sup>	−40	+85	°C	-
Relative humidity	RH	Capacitive <sup>29</sup>	0	100	%	-
Free corrosion current	$I_c$	LPR <sup>31</sup>	0.005	100	μA	20 mV

(AISI 1008) free corrosion sensor. This panel underwent surface preparation by cleaning with ethanol, sweep blasting using non-metallic grit, before the entire panel was coated with ~300 μm (DFT) commercial epoxy mastic by airless spray application. A crosscut across the corrosion sensor was made using a utility knife, as Fig. 14 shows. Precipitation and wind were measured with 60 minutes resolution.

This paper does not discuss the performance of the coating but focuses only on the corrosion in the scribe, trying to correlate that to the weather parameters. In addition, since the coating did not degrade notably during the 1-year exposure, the exposed area of the corrosion sensor remained almost constant and for the level of accuracy in this study, the degradation of the coating was negligible. Nevertheless, the sensor was exposed for several months before the reported logging period. Hence, the corrosion reported here does not include the high initial corrosion rates. A rust layer was already formed in October 2020 when the logging reported here started. Formation of more corrosion products during the period of the study reduced the corrosion rate further, as must be the case in any investigation of this kind. The data set that is reported here, October 2020 to October 2021, is the first 1-year set of continuous data. The discontinuous data have not been included in this study because that would bias the seasonal effects, but they showed similar measurements and trends to the ones reported here.

Table 1 shows a list of the parameters measured by the CorRES sensor and applied in this study. The manufacturer of the sensor panels has not provided any information about calibration, resolution, or drift of the sensors, so the reported data cannot be regarded as quantitatively accurate. The data are within the expected range and correlate well with other sources weather data, so for the purposes of this paper, the data have sufficient level accuracy.

## DATA AVAILABILITY

The data that support the findings of this study are available from Jotun AS but restrictions apply to the availability of these data, which were used under license for the current study, and so are not publicly available. Data are however available from the authors upon reasonable request and with permission of Jotun AS.

Received: 30 October 2022; Accepted: 25 January 2023;

Published online: 15 February 2023

## REFERENCES

- Morcillo, M., Chico, B., Díaz, I., Cano, H. & De la Fuente, D. Atmospheric corrosion data of weathering steels, a review. *Corros. Sci.* **77**, 6–24 (2013).
- Knudsen, O. Ø., Matre, H., Dørum, C. & Gagné, M. Experiences with thermal spray zinc duplex coatings on road bridges. *Coatings* **9**, 371 (2019).
- Fielding, T. ISO 12944: recent revisions. *J. Prot. Coat. Linings* **37**, 36–38 (2020).
- Diamantino, T. C., Gonçalves, R., Nunes, A., Páscoa, S. & Carvalho, M. J. Durability of different selective solar absorber coatings in environments with different corrosivity. *Sol. Energy Mater. Sol. Cells* **166**, 27–38 (2017).
- Corvo, F. et al. Time of wetness in tropical climate: considerations on the estimation of TOW according to ISO 9223 standard. *Corros. Sci.* **50**, 206–219 (2008).
- Li, Q. et al. Long-term corrosion monitoring of carbon steels and environmental correlation analysis via the random forest method. *NPJ Mater. Degrad.* **6**, 1–9 (2022).
- Morcillo, M. et al. On the mechanism of rust exfoliation in marine environments. *J. Electrochem. Soc.* **164**, C8 (2016).

- Chico, B., De la Fuente, D., Díaz, I., Simancas, J. & Morcillo, M. Annual atmospheric corrosion of carbon steel worldwide. An integration of ISOCORRAG, ICP/UNECE and MICAT databases. *Mater.* **10**, 601 (2017).
- Alcántara, J., Chico, B., Díaz, I., De la Fuente, D. & Morcillo, M. Airborne chloride deposit and its effect on marine atmospheric corrosion of mild steel. *Corros. Sci.* **97**, 74–88 (2015).
- Yan, L., Diao, Y., Lang, Z. & Gao, K. Corrosion rate prediction and influencing factors evaluation of low-alloy steels in marine atmosphere using machine learning approach. *Sci. Technol. Adv. Mater.* **21**, 359–370 (2020).
- Morcillo, M., Chico, B., De la Fuente, D. & Simancas, J. Looking back on contributions in the field of atmospheric corrosion offered by the MICAT iber-american testing network. *Int. J. Corros.* **2012**, 824365 (2012).
- Odnevall, W. I. & Leygraf, C. A critical review on corrosion and runoff from zinc and zinc-based alloys in atmospheric environments. *Corrosion* **73**, 1060–1077 (2017).
- Alcántara, J. et al. Marine atmospheric corrosion of carbon steel: a review. *Mater.* **10**, 406 (2017).
- de la Fuente, D. et al. Corrosion mechanisms of mild steel in chloride-rich atmospheres. *Corros* **67**, 227–238 (2017).
- Morcillo, M., Chico, B., Mariaca, L. & Otero, E. Salinity in marine atmospheric corrosion: its dependence on the wind regime existing in the site. *Corros. Sci.* **42**, 91–104 (2000).
- Feliu, S., Morcillo, M. & Chico, B. Effect of distance from sea on atmospheric corrosion rate. *Corrosion* **55**, 883–891 (1999).
- Escobar, L. A. & Meeker, W. Q. A review of accelerated test models. *Stat. Sci.* **21**, 552–577 (2006).
- Beysens, D. The formation of dew. *Atmos. Res.* **39**, 215–237 (1995).
- Mikhailov, A., Tidblad, J. & Kucera, V. The classification system of ISO 9223 standard and the dose–response functions assessing the corrosivity of outdoor atmospheres. *Prot. Met.* **40**, 541–550b (2004).
- Lawrence, M. G. The relationship between relative humidity and the dewpoint temperature in moist air: a simple conversion and applications. *Bull. Am. Meteorol. Soc.* **86**, 225–234 (2005).
- Benesty, J., Chen, J., Huang, Y. & Cohen, I. *Noise Reduction In Speech Processing* 37–41 (Springer 2009).
- Cai, Y., Xu, Y., Zhao, Y. & Ma, X. Atmospheric corrosion prediction: a review. *Corros. Rev.* **38**, 299–321 (2020).
- Cai, Y., Zhao, Y., Ma, X., Zhou, K. & Chen, Y. Influence of environmental factors on atmospheric corrosion in dynamic environment. *Corros. Sci.* **137**, 163–175 (2018).
- Lapuerta, S. et al. The influence of relative humidity on iron corrosion under proton irradiation. *J. Nucl. Mater.* **375**, 80–85 (2008).
- Cole, I. S., Ganther, W., Sinclair, J., Lau, D. & Paterson, D. A. A study of the wetting of metal surfaces in order to understand the processes controlling atmospheric corrosion. *J. Electrochem. Soc.* **151**, B627 (2004).
- Richter, D. H. & Veron, F. Ocean spray: An oversized influence on weather and climate. *Phys. Today* **69**, 34–39 (2016).
- Nyrkova, L., Osadchuk, S., Rybakov, A., Mel'nychuk, S. & Hapula, N. Investigation of the atmospheric corrosion of carbon steel under the conditions of formation of adsorption and phase moisture films. *J. Mater. Sci.* **48**, 687–693 (2013).
- Aas, W., Hjelbrekke, A. G., Fagerli, H., Benedictow, A. Deposition of major inorganic compounds in Norway 2012–2016 1–35, (Norwegian Institute for Air Research, 2017).
- Buxton, P. & Mellanby, K. The measurement and control of humidity. *Bull. Entomol. Res.* **25**, 171–175 (1934).
- Becker, J., Green, C. & Pearson, G. Properties and uses of thermistors—thermally sensitive resistors. *Electr. Eng.* **65**, 711–725 (1946).
- Friedersdorf, F. J., Demo, J. C., Brown, N. K., Kramer, P. C. Electrochemical sensors for continuous measurement of corrosion and coating system performance in outdoor and accelerated atmospheric tests, 91–113 (ASTM International, 2019).

## ACKNOWLEDGEMENTS

This work was financed by Bundesministerium für Wirtschaft und Klimaschutz, Germany (reference 03SX521B), Jotun AS, Research Council of Norway (reference 311714), and Vlaio, Belgium (reference HBC.2019.2654.) in a joint research project in the MarTERA program.

## AUTHOR CONTRIBUTIONS

B.D.: conceptualization, methodology, software, data curation, formal analysis, visualization, validation, writing—original draft, writing—review & editing. D.H.: funding acquisition, supervision, review & editing. O.Ø.K.: funding acquisition, conceptualization, project administration, supervision, investigation, writing—review & editing. A.W.B.S.: funding acquisition, resources, data curation. Review & editing.

## FUNDING

Open Access funding enabled and organized by Projekt DEAL.

## COMPETING INTERESTS

The authors declare no competing interests.

## ADDITIONAL INFORMATION

**Correspondence** and requests for materials should be addressed to Bahman Daneshian.

**Reprints and permission information** is available at <http://www.nature.com/reprints>

**Publisher's note** Springer Nature remains neutral with regard to jurisdictional claims in published maps and institutional affiliations.



**Open Access** This article is licensed under a Creative Commons Attribution 4.0 International License, which permits use, sharing, adaptation, distribution and reproduction in any medium or format, as long as you give appropriate credit to the original author(s) and the source, provide a link to the Creative Commons license, and indicate if changes were made. The images or other third party material in this article are included in the article's Creative Commons license, unless indicated otherwise in a credit line to the material. If material is not included in the article's Creative Commons license and your intended use is not permitted by statutory regulation or exceeds the permitted use, you will need to obtain permission directly from the copyright holder. To view a copy of this license, visit <http://creativecommons.org/licenses/by/4.0/>.

© The Author(s) 2023